Journal of Thermal Analysis and Calorimetry (2019) 135:2687–2695
https://doi.org/10.1007/s10973-018-7265-0

Rare earth compounds with 3-methoxybenzoic acid and terpyridine ligands

Structures, thermal and spectroscopic properties

Pan-Pan Shen[1,2] · Ning Ren[1] · Jian-Jun Zhang[2] · Xin-Fang Zheng[1]

Received: 1 January 2018 / Accepted: 4 April 2018 / Published online: 23 April 2018

Abstract
Two trivalent rare earth compounds $[Ln(3\text{-}MOBA)_3(terpy)(H_2O)]_2$ (Ln = Tb (**1**), Eu (**2**); 3-MOBA = 3-methoxybenzoate, terpy = 2,2′:6′,2″-terpyridine) were obtained in solid state, and the structure of **1** was determined by X-ray diffraction. The analysis of characterization was performed by elemental analysis, IR spectra, X-ray powder diffraction, thermogravimetric and differential scanning calorimetry coupled to infrared spectrometer (TG/DSC–FTIR). Besides that the luminescent properties and antibacterial activities were discussed. The crystal structure of **1** revealed that the asymmetric units were further stitched together to form 1D chain along the *x*-axis direction through the offset face-to-face $\pi\cdots\pi$ weak stacking interactions. Luminescence investigation revealed that compounds exhibited strong green and red emissions and the fluorescence quantum yield of two compounds were measured. What's more, the Commission Internationale de L'Eclairage chromaticity diagrams were presented. The antibacterial activity studies show that two compounds had good antibacterial actions on *E. coli*, *S. aureus* and no antibacterial activities on *C. albicans*.

Keywords Rare earth compounds · Crystal structure · Thermal properties · Luminescent properties · Antibacterial activities

Introduction

It is well known that the design and synthesis of aromatic carboxylic acids toward rare earth compounds have received considerable attention, due to their intriguing network topologies and promising applications in fields such as catalysis, ion exchange, gas storage, sensors, luminescence, antimicrobial [1–8]. Particularly, Eu(III) and Tb(III) ions could lead to interesting and excellent luminescence emissions in visible or near-infrared regions because the narrow $f \rightarrow f$ transitions derived from 4*f* electrons. Benzoic acid and its derivatives have a certain rigidity and stability in the structure. Their compounds with rare earth ions not only have a variety of interesting structures but also have good luminescence properties. At the same time, nitrogen heterocyclic ligands are introduced into the compounds of rare earth carboxylic acids, which can greatly improve the luminous intensity and thermal stability of the compounds [9–11]. Up to now, numerous one-dimensional (1D), two-dimensional (2D) and three-dimensional (3D) rare earth compounds have been synthesized with aromatic carboxylic acids and nitrogen heterocyclic ligands [12–15]. In addition, the research on the antibacterial activity of rare earth complexes is of great significance. For example, the compounds can selectively inhibit plant pathogenic bacteria and also have good bacteriostatic activity against *Candida albicans* [4].

In this report, two new rare earth compounds $[Ln(3\text{-}MOBA)_3(terpy)(H_2O)]_2$ (Ln = Tb (**1**), Eu (**2**); 3-MOBA = 3-methoxybenzoate, terpy = 2,2′:6′,2″-terpyridine) were synthesized. Two asymmetric dinuclear molecules and 1D

✉ Ning Ren
ningren9@163.com

✉ Jian-Jun Zhang
jjzhang6@126.com

[1] College of Chemical Engineering and Material, Handan University, Handan 056005, People's Republic of China

[2] Testing and Analysis Center, Hebei Normal University, Shijiazhuang 050024, People's Republic of China

chain along the *x*-axis direction of **1** are combined by the offset face-to-face $\pi\cdots\pi$ weak stacking interactions. In order to evaluate the thermal effect and thermal decomposition mechanism on the target compounds, thermogravimetric and differential scanning calorimetry coupled to infrared spectrometer (TG/DSC–FTIR) technology were performed. Additionally, the luminescent properties and antibacterial activities of the title compounds were investigated.

Experimental

Materials

$LnCl_3{\cdot}6H_2O$ was acquired by the reaction of Tb_4O_7 and Eu_2O_3, respectively (Ln = Tb, Eu, Beijing Lanthanide Innovation Technology Co., Ltd, 99.9%), and hydrochloric acid in aqueous solution. The other analytically pure chemicals were purchased and used without further purification.

Synthesis of $[Ln(3\text{-}MOBA)_3(terpy)(H_2O)]_2$ (Ln = Tb (1), Eu (2))

Dissolve 3-MOHBA (0.6 mmol) and terpy (0.2 mmol) in ethanol (95%) and adjust the pH of the solution about 6–7 with the prepared NaOH solution (1 mol L^{-1}). Add the mixed ligands solution to $LnCl_3{\cdot}6H_2O$ (0.2 mmol) aqueous solution under stirring. The precipitate was filtered off and washed with 95% ethanol and then dried. Elemental analysis: calcd. (%) for $C_{78}H_{68}Tb_2N_6O_{20}$: C 54.24, H 3.97, N 4.87, Tb 18.40; found (%): C 54.04, H 3.98, N 4.83, Tb 18.52. Calcd. (%) for $C_{78}H_{68}Eu_2N_6O_{20}$: C 54.68, H 4.00, N 4.91, Eu 17.74; found (%): C 54.22, H 3.97, N 4.94, Eu 17.57.

Physical measurements

Analyses for C, H, N were carried out on a Vario-EL II element analyzer. The IR spectra were measured in the range of 4000–400 cm^{-1} on a Bruker Tensor 27 spectrometer using KBr medium pellets. X-ray powder diffraction identification was carried out for the crystalline analyses by a D8 ADVANCE X-ray diffractometer in a scanning range of 5°–50° (2θ) with Cu K_α radiation (λ = 0.15418 Å, Bruker, Germany). The data of single-crystal X-ray diffraction were collected on a Smart-1000 diffractometer with graphite-monochromatic Mo K_α (λ = 0.71073 Å) for compounds **1** and **2** at 298(2) K. The structures were solved using the SHELXS-97 program and refined with full-matrix least squares on F^2 using the SHELXL-97 program. TG/DTG-FTIR analyses were carried out with 3–6 mg compounds at a heating rate of 10 K min^{-1} (simulated air atmosphere) on a NETZSCH STA 449 F3 instrument coupled with Bruker Tensor 27 Fourier transform infrared spectrometer. The luminescence spectra were measured on an F-4500 Hitachi Spectrophotometer. The solid luminescence quantum yields were measured using C9920-02G Hamamatsu test system, which was constituted by integrating sphere of 10-inch diameter and connected to a CCD detector. The antibacterial activities of $LnCl_3{\cdot}6H_2O$, ligands and the title compounds at 303.15 K were studied with four respective concentrations: 8×10^{-3}, 1.6×10^{-2} and 3.2×10^{-2} mol L^{-1} in sterile DMSO. The filter diameter is 6 mm, and the sample volume of the compounds is 5 μL.

Results and discussion

Infrared spectra

The absorption bands of 3-MOHBA, terpy and compounds **1**–**2** are listed in Table 1. The similar IR spectra of **1** and **2** suggest that the compounds are isostructural, which is further proved by the X-ray powder diffraction. The new characteristic bands of $\nu_{as(COO-)}$ and $\nu_{s(COO-)}$ for the title compounds are observed at 1536 cm^{-1} and 1402, 1401 cm^{-1}. The characteristic absorption band of $\nu_{C=O}$ (1691 cm^{-1}) for 3-MOHBA ligand disappeared in the IR spectra of the compounds. At the same time, the ν_{Ln-O} stretching vibration band of compounds is observed at 413 and 412 cm^{-1}. All of them indicate that oxygen atoms of the carboxylate groups are coordinated to the Ln(III) ions [16]. The bands $\nu_{C=N}$ and δ_{C-H} have shifted to higher wave numbers in the compounds compared to the free terpy ligand, proving that the nitrogen atoms of terpy ligand are also coordinated to the Ln(III) ion [17].

X-ray powder diffraction

The X-ray powder diffraction patterns have been measured at room temperature. The simulated curve of **1** and experimental curves of **1**–**2** are shown in Fig. 1. The experimental curve of **1** is almost in agreement with the simulated curve, showing that the structure of the powder of **1** is the same to the pure crystal. In addition, compounds 1–2 are isostructural due to the similar experimental curves [18].

Crystal Structure Description of $[Tb(3\text{-}MOBA)_3(terpy)(H_2O)]_2$

X-ray crystallographic data and structural refinement parameters for **1** are listed in Table 2. Compound **1** crystallizes in triclinic system, $P\bar{1}$ space group. There are two asymmetric dinuclear molecules in unit cell. They are

Table 1 IR absorption bands for the ligands and compounds

Ligand/compounds	$\nu_{C=N}/cm^{-1}$	δ_{C-H}/cm^{-1}	$\nu_{C=O}/cm^{-1}$	$\nu_{as(COO-)}/cm^{-1}$	$\nu_{s(COO-)}/cm^{-1}$	$\nu_{(Ln-O)}/cm^{-1}$
3-MOHBA	–	–	1691	–	–	–
Terpy	1580	831,764	–	–	–	–
1	1624	880,770	–	1536	1402	413
2	1623	879,766	–	1536	1401	412

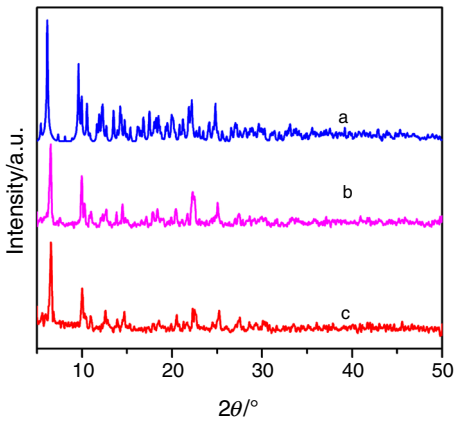

Fig. 1 Simulated and experimental XRD patterns of compounds (**a**: simulated pattern of **1**; **b**: experimental pattern of **1**; **c**: experimental pattern of **2**)

combined by the offset face-to-face π···π weak stacking interactions between terpy rings containing N1 and N5 of the neighboring dinuclear units, with the distance of 3.6175 Å. Each dinuclear unit in **1** consists of two Tb(III) ions, six 3-MOBA$^-$ ligands, two terpy molecules and two coordinated water molecules (Fig. 2a). Each Tb(III) ion is coordinated to nine atoms, of which five oxygen atoms are from the monodentate, bridging and bidentate chelating carboxylates, one oxygen atom is from the coordinated water molecule, and three nitrogen atoms are from terpy ligand. These nine atoms act in a distorted monocapped square antiprism (Fig. 2b) [19]. The bond lengths of Tb–O and Tb–N are listed in Table 3. The average distance of Tb1–O is 2.417(1) Å, which is shorter than that of Tb1–N bond of 2.619(5) Å. The average distance of Tb2–O is 2.414(1) Å, which is also shorter than that of Tb2–N bond of 2.601(5) Å. The 3-MOBA$^-$ ligands can be well coordinated with Tb(III) ion due to the electrostatic effects.

The asymmetric units are further connected to form 1D chain along the *x*-axis direction through the offset face-to-face π···π weak stacking interactions between terpy rings containing N2 and N4 on neighboring as shown in Fig. 3. The distance of the terpy rings is 3.5165 Å.

Table 2 Crystallographic data for compound **1**

Compound	**1**
Molecular formula	$C_{78}H_{68}Tb_2N_6O_{20}$
Formula weight/g mol^{-1}	1727.22
T/K	298(2)
Wavelength/Å	0.71073
Crystal system	Triclinic
Space group	$P\bar{1}$
a/Å	10.1640(9)
b/Å	16.5979(14)
c/Å	22.1471(19)
α/(°)	79.3400(10)
β/(°)	89.337(2)
γ/(°)	86.3050(10)
Volume/Å^3	3664.1(5)
Z, calculated density/Mg m^{-3}	2, 1.566
Absorption coefficient/mm^{-1}	1.993
F(000)	1736
Crystal size/mm^3	0.27 × 0.23 × 0.14
θ range for data collection/°	2.21–25.02
Limiting indices	$-10 \le h \le 12$
	$-19 \le k \le 14$
	$-26 \le l \le 26$
Reflections collected/unique	18,714/12,724 [$R_{(int)}$ = 0.0485]
Completeness to θ = 25.02°	98.4%
Max. and min. transmission	0.7678 and 0.6152
Data/restraints/parameters	12,724/0/961
Goodness of fit on F^2	1.081
R_1	0.0503
wR_2	0.1161
R_1 (all data)	0.0706
wR_2 (all data)	0.1238
Largest diff. peak and hole/(e·Å^{-3})	1.909 and − 1.736

The structure of **1** is similar to that of compound Tb(m-MOBA)$_3$(phen)]$_2$·2C$_2$H$_5$OH (m-MOBA = m-methoxybenzoate, phen = 1,10-phenanthroline) [20] and [Tb(4-EBA)$_3$(terpy)H$_2$O]$_2$ (4-EBA = 4-ethylbenzoate, terpy = 2,2′:6′,2″-terpyridine) [21]. The difference is that they both

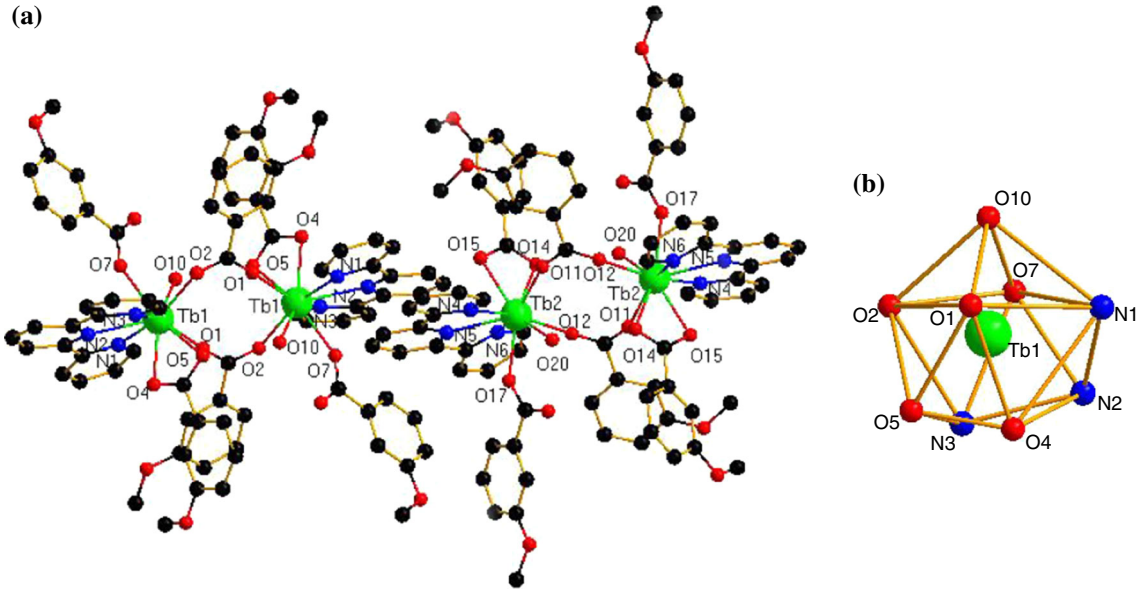

Fig. 2 **a** Crystal structure of **1** and **b** coordination geometry of Tb(III) ion

Table 3 Selected bond lengths (Å) of **1**

Bond	Length/Å	Bond	Length/Å
Tb(1)–O(1)	2.323(4)	Tb(2)–O(12)#2	2.307(4)
Tb(1)–O(7)	2.334(4)	Tb(2)–O(11)	2.321(4)
Tb(1)–O(2)#1	2.346(4)	Tb(2)–O(17)	2.370(4)
Tb(1)–O(4)	2.460(4)	Tb(2)–O(15)	2.488(4)
Tb(1)–O(10)	2.481(4)	Tb(2)–O(14)	2.496(4)
Tb(1)–O(5)	2.556(4)	Tb(2)–O(20)	2.500(4)
Tb(1)–N(3)	2.593(5)	Tb(2)–N(4)	2.584(5)
Tb(1)–N(1)	2.615(5)	Tb(2)–N(6)	2.595(5)
Tb(1)–N(2)	2.649(5)	Tb(2)–N(5)	2.624(5)

Symmetry transformations used to generate equivalent atoms: #1: $-x+1, -y+1, -z$; #2: $-x, -y, -z+1$

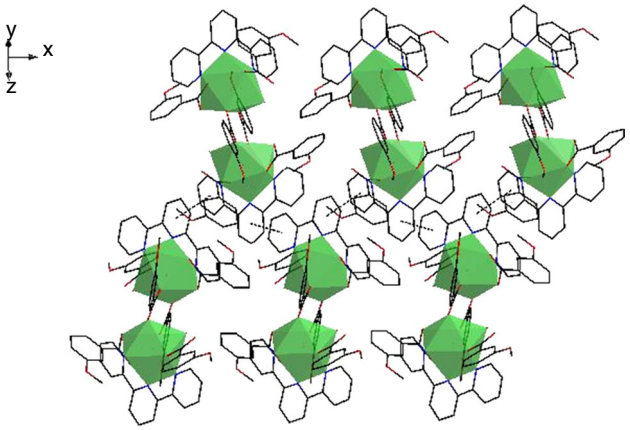

Fig. 3 1D chain structure along the *x*-axis

have one dinuclear molecule, which is different from **1**. Therefore, the choice of carboxylate ligands and nitrogenous heterocyclic ligands plays an important role in the structure regulation of the compound.

Thermal decomposition processes of the compounds

The TG/DTG-DSC methods were used to describe thermal decomposition of **1** and **2** in air, as shown in Fig. 4a, b. The thermal analytical data are listed in Table 4. The 3D stacked plots of FTIR spectra of gaseous products for **1** and **2** are shown in Figs. 5a and 6a. The IR spectra of the evolved gases of them at different temperature are performed in Figs. 5b and 6b. Their thermal behaviors are similar, so **1** would be described in detail as the representative.

In Fig. 4a, compound **1** has three decomposition steps, which is consistent with the FTIR spectra of the evolved gases (Fig. 5). The first step mass loss of 1.98% (calcd: 2.09%) between 339.15 and 453.15 K is attributed to the release of two coordinated water molecules. However, the gas signal is too weak to detect in this temperature range (Fig. 5a). In the temperature of 453.15–629.15 K, there is obvious mass loss of 26.94% (calcd.: 27.01%) corresponding to the decomposition of terpy ligands. Meanwhile, the weak absorption peaks of CO_2 are found in the range of 2404–2227 cm^{-1}, and some weak absorption peaks: $\nu_{(C=C)}$, 1594 cm^{-1}, $\nu_{(C=N)}$,1451 cm^{-1}, $\nu_{(C-H)}$, 2960 cm^{-1}, $\nu_{(C=O)}$, 1747 cm^{-1} are also observed in the IR spectra at 524.37 K. In the third stage, there is a mass loss of 49.48% (calcd.: 52.50%) in the temperature of

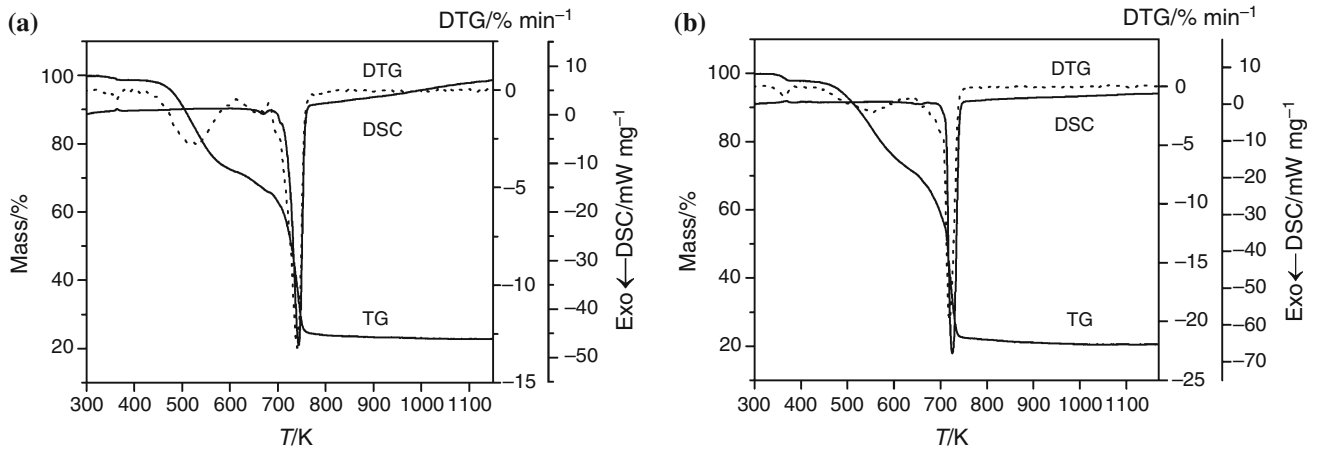

Fig. 4 TG/DTG/DSC curves of **1** (**a**) and **2** (**b**)

Table 4 Thermal analytical data for **1**–**2**

Compounds	Temperature range/K	T_p (DTG)/K	Mass loss rate/%		Probable expelled groups	Residue
			Found	Calculated		
1	339.15–453.15	361.85	1.98	2.09	$2H_2O$	$[Tb(3\text{-}MOBA)_3(terpy)]_2$
	453.15–629.15	527.45	26.94	27.01	2 terpy	$[Tb(3\text{-}MOBA)_3]_2$
	629.15–1064.15	740.55	49.48	52.50	6 (3-MOBA)	$1/2Tb_4O_7$
			78.40[a]	81.60[b]		
2	334.15–405.15	364.75	2.05	2.10	$2H_2O$	$[Eu(3\text{-}MOBA)_3(terpy)]_2$
	405.15–640.15	554.65	26.52	27.23	2 terpy	$[Eu(3\text{-}MOBA)_3]_2$
	640.15–970.15	719.25	50.60	52.93	6 (3-MOBA)	Eu_2O_3
			79.17[a]	82.26[b]		

[a]Experimental total weight loss rate

[b]Theoretical total weight loss rate

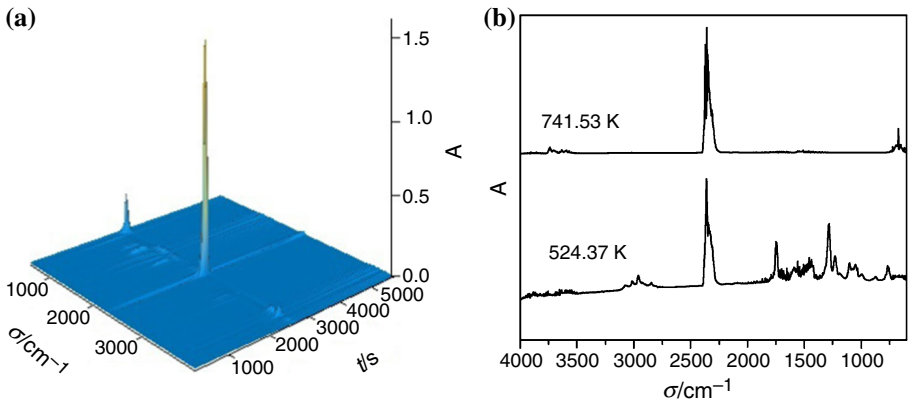

Fig. 5 3D stacked plots of the FTIR spectra of the evolved gases (**a**) and the FTIR spectra of the evolved gases (**b**) for **1**

629.15–1064.15 K, which belongs to the decomposition of the $3\text{-}MOBA^-$ ligands with the products of CO_2 (2403–2268 cm^{-1}, 668 cm^{-1}) and H_2O (3709–3535 cm^{-1}, 1783–1342 cm^{-1}), as shown in IR spectra at 741.53 K. Compound **1** is completely degraded into Tb_4O_7 with the mass loss of 78.40% (calcd.: 81.60%).

Luminescence

Solid-state luminescent spectra (at room temperature) of **1**–**2** are shown in Fig. 7a, b. Figure 8 shows Commission Internationale de L'Eclairage (CIE) chromaticity diagrams for two compounds.

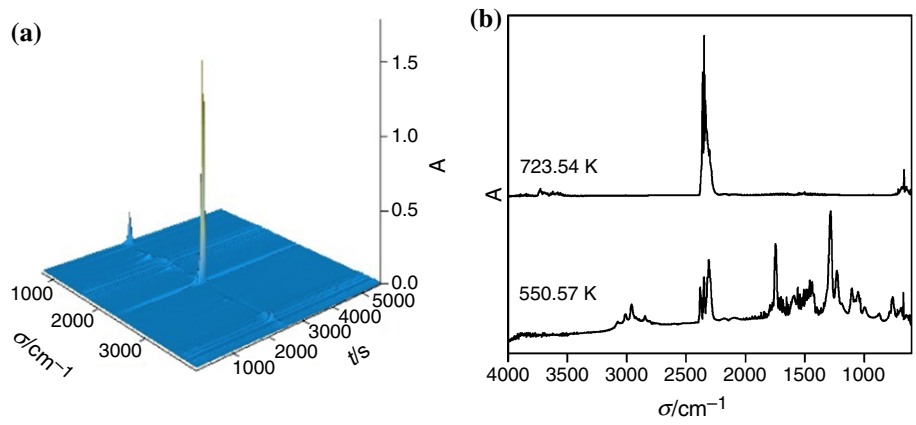

Fig. 6 3D stacked plots of the FTIR spectra of the evolved gases (**a**) and the FTIR spectra of the evolved gases (**b**) for **2**

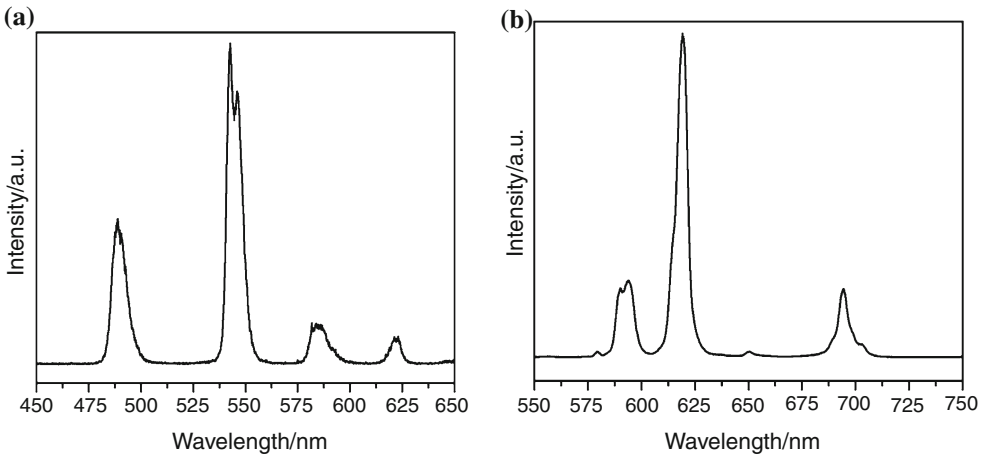

Fig. 7 **a** Emission spectra of **1** (λ_{ex} = 342 nm); **b** emission spectra of **2** (λ_{ex} = 345 nm)

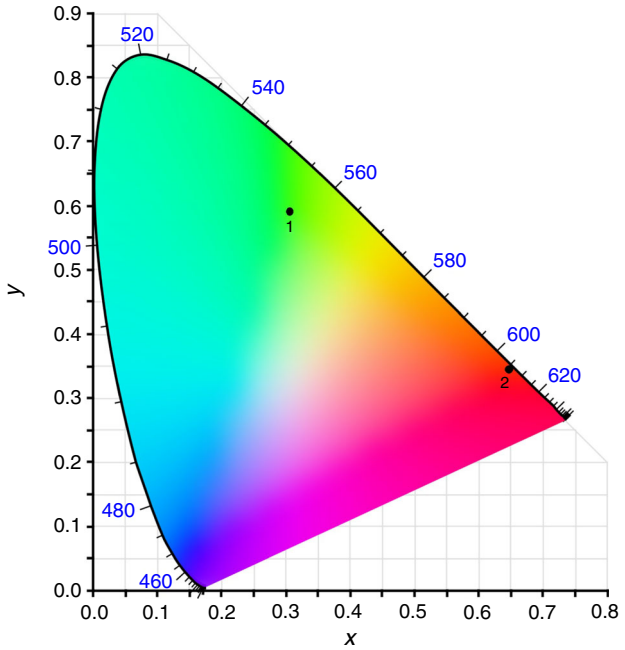

Fig. 8 CIE chromaticity diagrams of the two compounds (**1** = compound **1**; **2** = compound **2**)

As expected, compound **1** exhibits green emission with the typical bands of Tb(III) ion attributed to the electronic transitions $^5D_4 \rightarrow {}^7F_J$ (J = 6, 5, 4 and 3). The detailed CIE chromaticity coordinate values are (0.282, 0.590). The four characteristic emission bands of **1** are at 489, 543, 584 and 623 nm, respectively. The ligand-based emissions are not observed, indicating that the effective sensitization is from the ligands to the central Tb(III) ion under photoluminescence [22, 23]. The hypersensitive transition ($^5D_4 \rightarrow {}^7F_5$) at 543 nm is the most intense transition, which dominates the characteristic green fluorescence of terbium complex. Furthermore, the $^5D_4 \rightarrow {}^7F_5$ transition is the strongest among the four bands, and the fluorescent quantum yield is 0.851 (λ_{ex} = 342 nm). These indicate that the ligands are suitable for the sensitization of green fluorescence for Tb(III) ion at room temperature.

As shown in Fig. 8, the CIE chromaticity coordinate values of compound 2 are (0.643, 0.357) and "red" emission is emitted. Transitions from the excited $^5D_0$ state to the different J (0–4) levels of the lower ^7F_J state are observed in the range of 500–700 nm. The emission bands at 579 and 652 nm are very weak since their corresponding transitions $^5D_0 \rightarrow {}^7F_0$ and $^5D_0 \rightarrow {}^7F_3$ are forbidden in both

Table 5 Antibacterial activities of ligands and compounds with three different concentrations at 303.15 K

	Ligand/compounds	Diameter of bacteriostatic ring for three times in parallel/mm								
		8×10^{-3}/mol L^{-1}			1.6×10^{-2}/mol L^{-1}			3.2×10^{-2}/mol L^{-1}		
		I	II	III	I	II	III	I	II	III
Escherichia coli	DMSO	6.00	6.00	6.00	6.00	6.00	6.00	6.00	6.00	6.00
	3-MOHBA	6.00	6.00	6.00	6.00	6.00	6.00	6.00	6.00	6.00
	Terpy	6.00	6.00	6.00	6.00	6.00	6.00	12.20	11.70	11.50
	1	7.80	7.80	7.20	12.10	13.70	12.70	16.00	15.60	15.80
	2	6.00	6.00	6.00	11.90	13.00	12.10	17.70	17.30	17.90
Staphylococcus aureus	DMSO	6.00	6.00	6.00	6.00	6.00	6.00	6.00	6.00	6.00
	3-MOHBA	6.00	6.00	6.00	6.00	6.00	6.00	6.00	6.00	6.00
	Terpy	6.00	6.00	6.00	6.00	6.00	6.00	12.40	12.40	12.10
	1	6.00	6.00	6.00	9.00	9.30	9.63	15.00	15.40	15.53
	2	6.00	6.00	6.00	8.60	9.60	9.63	17.30	16.50	16.73

magnetic dipole and electric dipole fields. Two lines splitting for the $^5D_0 \rightarrow {}^7F_1$ transition at 594 nm suggest the axial symmetry exists [24, 25]. The hypersensitive transition $^5D_0 \rightarrow {}^7F_2$ at 619 nm is the most intense transition, which dominates the whole emission spectra, leading to the characteristic red fluorescence of Eu(III) complex. The emission of Eu(III) ion often used as a sensitive probe to investigate the local environment around the ions [26]. The energy transfer from the ligands to the Eu(III) ion by intersystem crossing is efficient, which is probably attributed to the matching of energy levels between excited states of ligands and excited states of Eu(III) ion. Further, the fluorescent quantum yield is 0.441. All above prove that 3-$MOBA^-$ and terpy ligands are good chromophore to absorb energy and transfer to Eu(III) ion, and emit the characteristic fluorescence of Eu(III) ion.

Two compounds both exhibit excellent fluorescence. The quantum yield of the two complexes shows that the fluorescence property of the terbium compound is stronger than that of the europium compound. Hence, the title compounds have potential application value as luminescent material.

Antibacterial activities

The antibacterial activities of ligands and compounds for *C. albicans* (fungus), *Escherichia coli* and *Staphylococcus aureus* (bacteria) were determined using the filter paper disk diffusion method at 303.15 K. The ligands and compounds were, respectively, dissolved in DMSO solutions at different concentrations of 8×10^{-3}, 1.6×10^{-2} and 3.2×10^{-2} mol L^{-1}. The experimental results show that 3-MOHBA ligand has no antibacterial action on *C. albicans*, *E. coli* and *S. aureus*, while the two compounds and terpy ligand exerted good antibacterial activity on *E. coli* and *S. aureus* but no antibacterial action on *C. albicans*, which may be attributed to the selective inhibitions of the compounds and ligands on antibacterial species. As shown in Table 5, the antibacterial actions of compounds and terpy ligand are more and more remarkable with the increase in the concentration in the range of tested concentrations.

In short, Ln(III) ions are coordinated with the donor atoms of the ligands, which make them have certain antibacterial activities on microorganism. The π-electron delocalization over the chelate ring further reduces the polarity of the central metal cation and increases the lipophilicity [27]. The bacteriostatic mechanism of the compounds is presumably that they have a good lipophilic nature arising from chelation.

Conclusions

The synthesis and characterization of two new compounds have been successfully reported. IR spectra and X-ray powder diffraction indicate that compounds **1–2** are isostructural. The crystal structure of **1** has two asymmetric dinuclear molecules in unit cell, and each Tb(III) ion is nine coordinated. The asymmetric units are further connected to form 1D chain along the *x*-axis direction through the offset face-to-face $\pi\cdots\pi$ weak stacking interactions. The thermal decomposition mechanisms of the compounds are obtained by TG/DSC-FTIR techniques. The FTIR spectra of the evolved gases show that the carboxylic ligands are completely decomposed, which is consistent with the TG analysis. What's more, the terbium and europium compounds exhibit excellent fluorescence. The antibacterial

performance study shows that two compounds have good antibacterial actions on *E. coli* and *S. aureus*.

Supporting information

The number of compound **1** CCDC 1557510 contains the supplementary crystallographic data for this paper, which can be obtained free of charge from the Cambridge Crystallographic Data Centre via www.ccdc.cam.ac.uk/data_request/cif.

Acknowledgements The research work was supported by the National Natural Science Foundation of China (No. 21473049), the Natural Science Foundation of Hebei Province (No. B2016205207) and Science and Technology Program of Handan (No. 1621202043-2).

References

1. Zhang S, Yang Y, Xia ZQ, Liu XY, Yang Q, Wei Q, Xie G, Chen SP, Gao SL. Eu-MOFs with 2-(4-carboxyphenyl)imidazo[4,5-f]-1,10-phenanthroline and ditopic carboxylates as coligands: synthesis, structure, high thermostability, and luminescence properties. Inorg Chem. 2014;53(20):10952–63.
2. Song XZ, Song SY, Qin C, Su SQ, Zhao SN, Zhu M, Hao ZM, Zhang HJ. Syntheses, structures, and photoluminescent properties of coordination polymers based on 1,4-bis(imidazol-l-yl-methyl)benzene and various aromatic dicarboxylic acids. Cryst Growth Des. 2012;12:253–63.
3. Onodera H, Nakajima A, Nakanishi T, Fushimi K, Hasegawa Y. Thermostable Eu(III)-nanorod luminophores with effective photosensitized energy transfer. J Alloys Compd. 2015;648:651–7.
4. Wang Y, Jin CW, He SM, Ren N, Zhang JJ. Five novel lanthanide compounds with 2-chloroquinoline-4-carboxylic acid and 1,10-phenanthroline: crystal structures, molecular spectra, thermal properties and bacteriostatic activities. J Mol Struct. 2016;1125:383–90.
5. Li QF, Yue D, Ge GW, Du X, Gong Y, Wang Z, Hao J. Water-soluble $Tb^{(3+)}$ and $Eu^{(3+)}$ complexes based on task-specific ionic liquid ligands and their application in luminescent poly(vinyl alcohol) films. Dalton Trans. 2015;44:16810–7.
6. Ren YL, Wang F, Hu HM, Chang Z, Yang ML, Xue G. Lanthanide coordination compounds with 2,2′-bipyridine-6,6′-dicarboxylate: synthesis, crystal structure, luminescence and magnetic property. Inorg Chim Acta. 2015;434:104–12.
7. Li HN, Li HY, Li LK, Xu L, Hou K, Zang SQ, Mak TCW. Syntheses, structures, and photoluminescent properties of lanthanide coordination polymers based on a zwitterionic aromatic polycarboxylate ligand. Cryst Growth Des. 2015;15:4331–40.
8. Bai FH, Wen D, Gao YJ, Zhang LP, Suo YJ, Su HQ. A series of supramolecular complexes constructed from discrete lanthanide dinuclear butterfly-shaped clusters: syntheses, structures and properties. Inorg Chem Commun. 2017;86:70–3.
9. Matias FRM, da Silva VMF, Nunes RS, Luiz JM. Synthesis, characterization and thermal behavior of some trivalent lanthanide 4-amino-benzenesulfonate salts. J Therm Anal Calorim. 2017;130:2185–90.
10. Feng SY, Li WX, Zheng YS, Xin XD, Guo F, Cao XF. Syntheses and luminescence properties of two novel lanthanide(III) perchlorate compounds with phenacyl *p*-tolyl sulfoxide. J Lumin. 2015;162:92–6.
11. Wang Y, Zhao QQ, Ren N, Zhang JJ, Geng LN, Wang SP. Crystal structures, thermal properties, and luminescent properties of two novel mononuclear lanthanide compounds with 2,4-dichlorobenzoic acid and 2,2′:6′,2″-terpyridine. J Therm Anal Calorim. 2016;126:1703–12.
12. Feng R, Jiang FL, Wu MY, Chen L, Yan CF, Hong MC. Structures and photoluminescent properties of the lanthanide coordination complexes with hydroxyquinoline carboxylate ligands. Cryst Growth Des. 2010;10(5):2306–13.
13. Pitchaimani P, Lo KM, Elango KP. Synthesis, crystal structures, luminescence properties and catalytic application of lanthanide(III) piperidine dithiocarbamate complexes. Polyhedron. 2015;93:8–16.
14. Fu RB, Hu SM, Wu XT. New 3D lanthanide phosphonates: syntheses, crystal structure, thermal stability, luminescence, and magnetism. Cryst Growth Des. 2014;14:6197–204.
15. Chen XL, Li CC, Ai FF, Qu X, Liu K. Syntheses, crystal structures, and luminescence of two lanthanide coordination polymers based on 5-(3′,4′-bis(tetrazol-5″-yl)phenoxy)isophthalic acid and 1,10-phenanthroline. J Mol Struct. 2017;1133:369–73.
16. Zhao QQ, Ren N, Zhang JJ, Geng LN, Wang SP, Shi SK. Three novel Ho(III) complexes with different auxiliary ligands: synthesis, crystal structures and thermal properties. Polyhedron. 2017;132:78–89.
17. Wang Y, Shen PP, Ren N, Zhang JJ, Geng LN, Wang SP, Shi SK. A series of lanthanide compounds with different N-donor ligands: synthesis, structures, thermal properties and luminescence behaviors. RSC Adv. 2016;6:70770–80.
18. Wu JC, Jin CW, Zhang DH, Ren N, Zhang JJ. A series of lanthanide compounds with 2,3-dichlorobenzoic acid and 2,2:6′,2″-terpyridine: crystal structures, spectroscopic and thermal properties. Thermochim Acta. 2015;620:28–35.
19. King RB, Silaghi-Dumitrescu I. Density functional theory study of nine-atom germanium clusters: effect of electron count on cluster geometry. Inorg Chem. 2003;42:6701–8.
20. Ma RX, Chen ZM, Gao ZH, Wang SP, Wang RF, Zhang JJ. Synthesis, structures and properties of ternary rare earth compounds with m-methoxybenzoic acid and 1,10-phenanthroline. Synth Met. 2009;159:1272–6.
21. Huo JX, Wang Y, Zhang DH, Ren N, Zhang JJ. Syntheses, characterization, luminescence, and thermal decomposition mechanism of four lanthanide compounds with 4-ethylbenzoic acid and terpyridine. J Therm Anal Calorim. 2016;124:1575–85.
22. Hou XY, Wang X, Gao LJ, Fu F, Wang JJ, Cao J. Synthesis, structures, luminescence, and magnetic properties of two three-dimensional lanthanide organic frameworks comprising pyrazine-2,3-dicarboxylic acid. Z Anorg Allg Chem. 2014;640:2072–7.
23. Ramya AR, Reddy ML, Cowley AH, Vasudevan KV. Synthesis, crystal structure, and photoluminescence of homodinuclear lanthanide 4-(dibenzylamino)benzoate compounds. Inorg Chem. 2010;49:2407–15.
24. You LX, Wang SJ, Xiong G, Ding F, Meert KW, Poelman D, Smet PF, Ren BY, Tian YW, Sun YG. Synthesis, structure and properties of 2D lanthanide coordination polymers based on N-heterocyclic arylpolycarboxylate ligands. Dalton Trans. 2014;43:17385–94.
25. Liu TF, Zhang W, Sun WH, Cao R. Conjugated ligands modulated sandwich structures and luminescence properties of lanthanide metal–organic frameworks. Inorg Chem. 2011;50:5242–8.
26. Oliveira CK, de Souza VP, da Luz LL, de Menezes Vicenti JR, Burrow RA, Severino A, Longo RL, Malvestiti I. Synthesis,

crystal structure and luminescent properties of lanthanide extended structure with asymmetrical dinuclear units based on 2-(methylthio)benzoic acid. J Lumin. 2016;170:528–37.
27. Zhao YF, Chu HB, Bai F, Gao DQ, Zhang HX, Zhou YS, Wei XY, Shan MN, Li HY, Zhao YL. Synthesis, crystal structure, luminescent property and antibacterial activity of lanthanide ternary compounds with 2,4,6-tri(2-pyridyl)-s-triazine. J Organomet Chem. 2012;716:167–74.